

**Georgia Institute
of Technology**



**Determination of Interlaminar Toughness of IM7/977-2
Composites at Temperature Extremes and Different
Thicknesses**

Final Report

***NASA Grant Number: NAG-1-02003
Ga Tech Project Number E-18-A19***

***W. S. Johnson, Ph.D.
M. M. Pavlick, M. S. Oliver***

**Georgia Institute of Technology
Atlanta, GA 30332-0245**

May 2005

Determination of Interlaminar Toughness of IM7/977-2 Composites at Temperature Extremes and Different Thicknesses

M. M. Pavlick¹, M. S. Oliver², W. S. Johnson, Ph.D. ^{1,2,*}

¹ George W. Woodruff School of Mechanical Engineering, Georgia Institute of Technology, Atlanta, GA 30332

² School of Materials Science and Engineering, Georgia Institute of Technology, Atlanta, GA 30332

* Corresponding author

Abstract

Composite materials are being used in the aerospace industry as a means of reducing vehicle weight. In particular, polymer matrix composites (PMC) are good candidates due to their high strength-to-weight and high stiffness-to-weight ratios. Future reusable space launch vehicles and space exploration structures will need advanced light weight composites in order to minimize vehicle weight while demonstrating robustness and durability, guaranteeing high factors of safety. In particular, the implementation of composite cryogenic propellant fuel tanks (cryotanks) for future reusable launch vehicles (RLVs) could greatly reduce the vehicle's weight versus identically sized cryotanks constructed of metallic materials.

One candidate composite material for future cryotank designs is IM7/977-2, which is a graphite/epoxy system. A successful candidate must demonstrate reasonable structural properties over a wide range of temperatures. Since the matrix material is normally the weak link in the composite, tests that emphasize matrix-dominated behavior need to be conducted. Therefore, the objective of this work is to determine the mode I interlaminar fracture toughness of "unidirectional" 8-ply and 16-ply IM7/977-2 through experimental testing. Tests were performed at -196 °C (-320 °F), 22 °C (72 °F), 93 °C (200 °F) and 160 °C (320 °F). Low temperature testing was completed while the specimen was submerged in a liquid nitrogen bath. High temperature testing was completed in a temperature-controlled oven.

Keywords: cryogenic, cryotank, interlaminar fracture toughness, composites, thickness effects

1. Introduction

In an effort to reduce the operating costs of future reusable launch space vehicles, recent research has been focused on the reduction of structural weight. The internal propellant tanks are often the largest component in a single-stage-to-orbit (SSTO) vehicle and consume the bulk weight of the vehicle. PMCs offer a significant weight savings compared to metals in cryotank designs. For example, the DC-XA with a graphite/epoxy tank was approximately 544 kg (1200 lb) lighter than a similar aluminum tank used in the DC-X [1].

During a typical RLV flight cycle, cryotank temperatures can vary from 250 °C (-420 °F) when the cryotanks are full of propellant to over 125 °C (260 °F) during re-entry with empty tanks depending upon the amount of thermal protection system used. This large temperature variation will cause significant thermal stresses throughout the layers of the composite. Overall stresses in the material are from flight loads combined with thermally induced stresses. It is important to understand the material's stress-carrying capability at all operational temperatures. In addition to carrying stress, the structure must not leak. Therefore, the candidate composite materials must still be able to absorb energy and prevent cracking, even at these extreme temperatures and loading conditions. The cracking that would lead to leakage and delamination is controlled by the matrix material's properties: in particular, the matrix material's toughness. One way of assessing the matrix's ability to resist cracking is to measure the interlaminar fracture toughness of the composite. Thus is the purpose of this paper, to assess the interlaminar fracture toughness

of IM7/977-2 over a rather large temperature range using double cantilever beam (DCB) specimens. The effect of the number of plies in the DCB specimen will also be addressed.

2. Materials

The carbon/epoxy composite IM7/977-2 was the material examined in this research. IM7 is a continuous, intermediate modulus, PAN-based fiber manufactured by Hexcel [2]. 977-2 is a toughened epoxy resin manufactured by Cycom [3].

The goal of testing two panels with different thicknesses was to examine if the interlaminar fracture toughness (a material property) varies significantly at the extreme temperatures a cryotank must endure. Two different 30.48 cm x 30.48 cm (12 in x 12 in) IM7/977-2 panels were manufactured with the following layups: $[0_3/\pm 3/0_3]$ and $[0_7/\pm 3/0_7]$. As noted by Johnson & Mangaliri [4], the purpose of the ± 3 layer was to minimize fiber bridging. Between the ± 3 layers normal to the fiber direction, 3.81 cm (1.5 in) wide, two 5.2-mil thick Teflon strips were inserted to serve as an initial delamination. The panels were made by vacuum bagging and cured in an autoclave at Lockheed-Martin in Marietta, GA. The bagging and cure cycle procedures were completed according to Lockheed standards.

3. Experimental Testing

For optimal design purposes, it is essential to consider the material's resistance to ply cracking and delamination, along with its strength, as failure criterion. Therefore, the mode

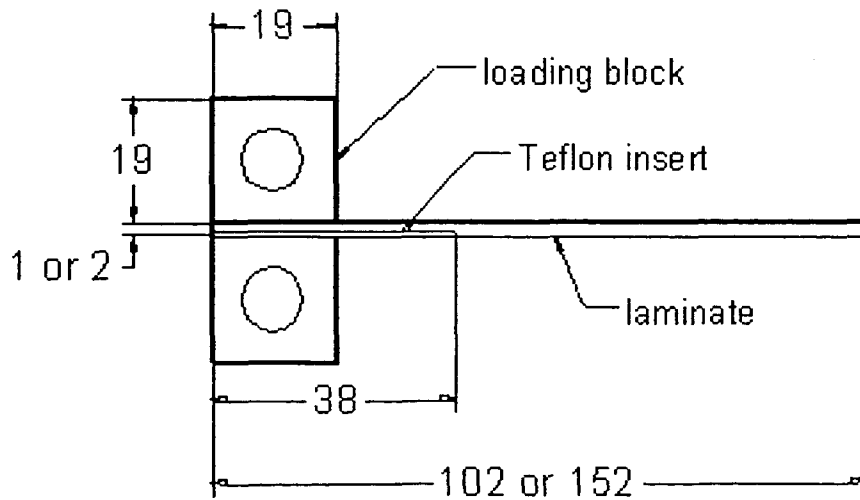
I interlaminar fracture toughness of IM7/977-2 was determined experimentally. Double cantilever beam (DCB) specimens were tested under displacement control at a rate of 5.08 mm/min (0.2 in/min) using a screw-driven test frame with a 4500-N (1000-lb) load cell. Testing was conducted at approximately -196 °C (-320 °F), 22 °C (72 °F), and 160 °C (320 °F). A few experiments at an intermediate elevated temperature, 93 °C (200 °F), using only 16-ply specimens were completed to verify interpolations between elevated and room temperatures. A temperature-controlled oven was used for high temperature testing, and a custom-designed chamber allowing specimens to be fully submerged in liquid nitrogen was used for low temperature testing.

3.1. Specimen Preparation

Approximately 20 specimens were cut from each unidirectional composite panel using a diamond saw. Each test specimen was approximately 2.54 cm (1 in) wide and either 10.16 cm (4 in) or 15.24 cm (6 in) long, depending upon the test conditions. The 10.16 cm (4 in) specimens were used for cryogenic and elevated temperature tests in order to fit in the respective chambers. The 15.24 cm (6 in) specimens were used at room temperature. One exception was: 15.24 cm (6 in) long test specimens were used for the 16-ply IM7/977-2 cryogenic specimens in order to be able to obtain more data points from a single experiment. A larger cryogenic box was constructed for the 16-ply tests.

Machined aluminum loading blocks were attached to each specimen as shown in Figure 1. At room temperature, an adhesive (MetlBond 1515-3M) manufactured by Cytec was used to bond the blocks to the specimens. At cryogenic and elevated temperatures, the

adhesive failed since its usage temperature range was exceeded. Therefore, two novel techniques were used for attaching the loading blocks to the specimens. For the 8-ply cryogenic specimens, two thin aluminum sleeves were inserted at the mid-plane of each specimen and bent around the loading blocks to help secure the blocks to the adhesive and composite specimen. As seen in Figure 2, this method required wedging the two thin sleeves into the mid-plane crack created by the Teflon. This procedure was completed with extreme caution as to not make an initial crack beyond the Teflon flaw. For the 16-ply cryogenic and elevated temperature specimens, each composite specimen and loading blocks were machined as to have bolts pass through counter-sunk holes in the loading blocks and $\frac{1}{2}$ the thickness of the composite specimen and then be secured into a threaded hole in the loading block on the opposite side. This method is identical to the one used by Melcher *et al.* [5] and is shown in Figure 3.



All units are in mm

Fig. 1. Double cantilever beam specimen dimensions

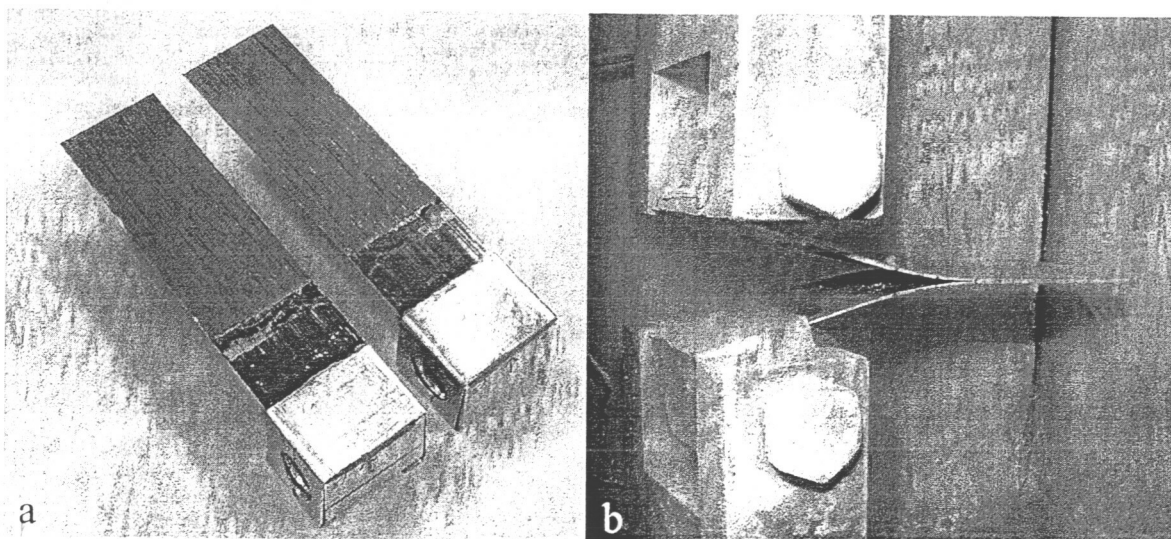


Fig. 2. (a) Special “U-clip” loading block design for 8-ply cryogenic specimen testing.

(b) 8-ply IM7/977-2 specimen during cryogenic testing

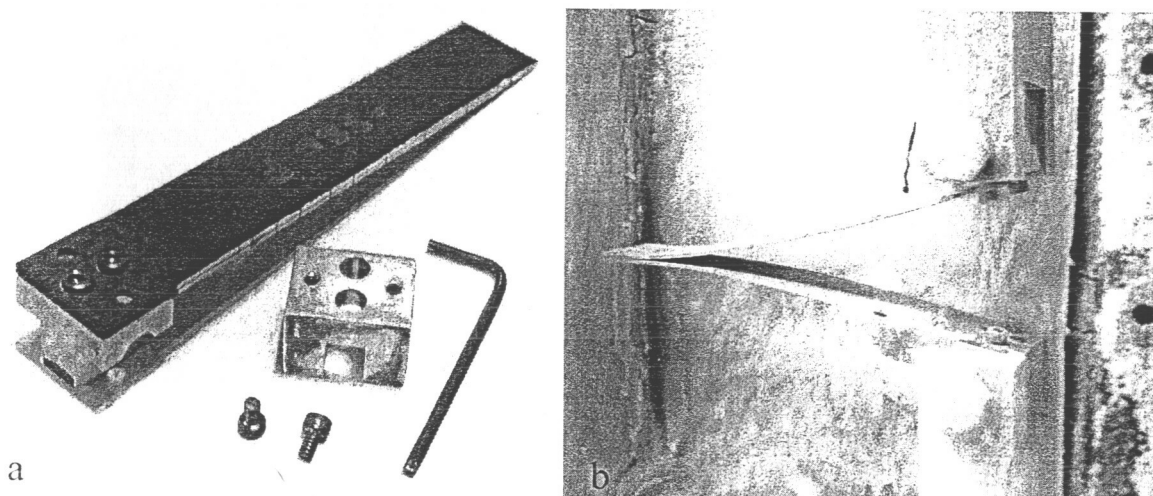


Fig. 3. (a) Special bolted loading block design for 16-ply elevated and cryogenic specimen testing.

(b) 16-ply IM7/977-2 specimen during cryogenic testing

The edges of each specimen were painted white so that the crack tip could be identified more easily. Since the test software could only measure load vs. displacement in real time, crack length was measured manually with the aid of a magnifying glass. This was achieved

by pausing the test when a load drop occurred, then marking the crack length with a permanent fine-tip pen.

3.2. Equipment and Environmental Exposure

For cryogenic testing, specimens were fully submerged into a liquid nitrogen (LN₂) bath in a custom-made environmental chamber as shown in Figure 4. Once a specimen was secured in the clevises and the load was zeroed, gaseous nitrogen was added prior to LN₂ to avoid thermal shock to the specimen. After approximately 20-30 minutes, the entire system reached LN₂ equilibrium, which was measured by using digital thermometers and T-type thermocouples. Due to thermal contraction during the cooling cycle, the test frame's crosshead had to be lowered until the load read zero. Therefore, once equilibrium was met and the initial load was zero, testing could commence. A similar procedure for elevated temperature exposure was followed using a temperature-controlled oven. However, due to thermal expansion, the crosshead had to be raised in order to tare the load.

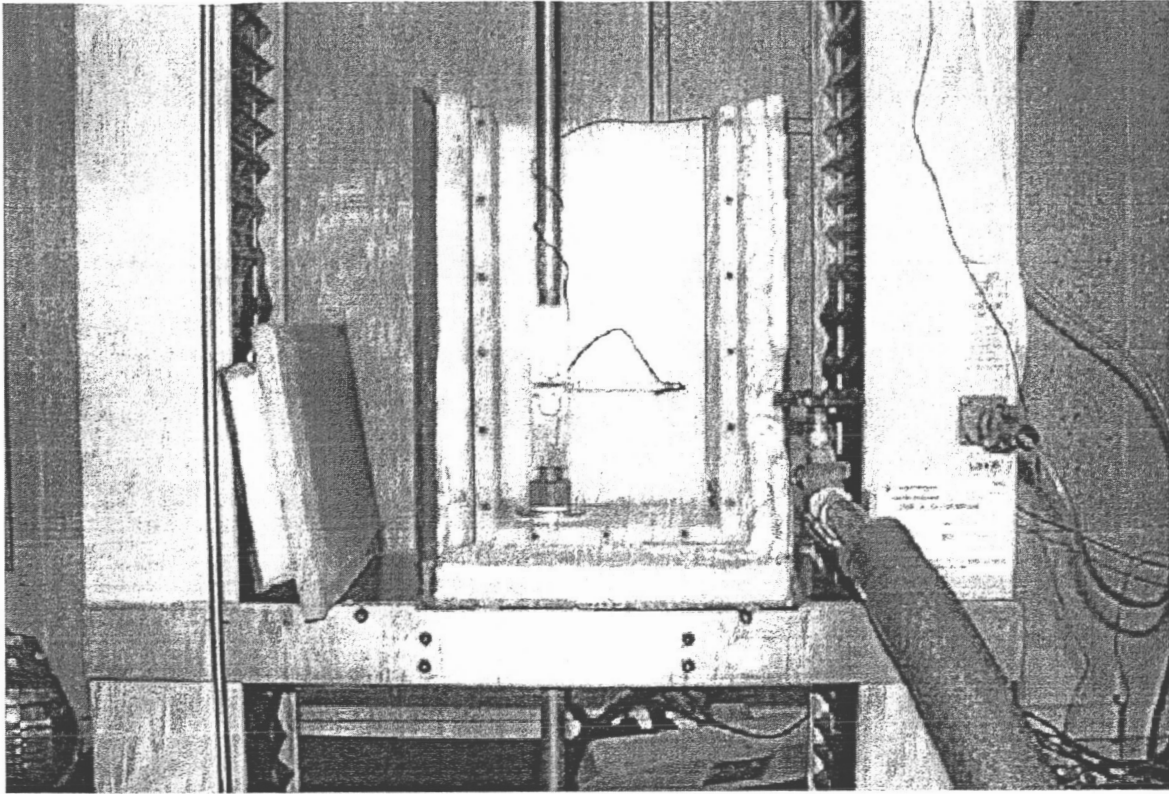


Fig. 4. Cryogenic test chamber. Notice the DCB test specimen with a thermocouple attached.

3.3. Double Cantilever Beam Testing

Experimental testing was conducted at a displacement rate of 5.08 mm/min (0.2 in/min) using a screw-driven test frame with a 4450-N (1000-lb) load cell. Specimens were loaded until unstable crack growth was observed, which was indicated by a drop in the load-displacement curve. Upon the initiation of unstable crack growth, the test was paused and the crack was allowed to relax. While the test was paused and with the aid of a magnifying glass, the location of the crack tip along the edge of the specimen was marked by hand with a permanent pen. Then the specimen was unloaded to approximately 4.45 N (1.0 lb) before

loading was started again. This procedure was repeated for several crack growth increments or until the specimen failed.

For cryogenic testing, the procedure became more complicated. The environmental chamber had to be fully drained prior to removing the front face and marking the crack length. Once the crack was marked and the front face of the environmental chamber was secured again, the drain valve was closed and gaseous nitrogen was pumped into the chamber prior to liquid nitrogen. Unloading could occur while the chamber was refilling, however, the loading cycle could not begin until the specimen was completely submerged again. Because of the environmental chamber design, crack length could only be measured on one side of the specimen.

For elevated temperature testing, a similar procedure as cryogenic testing was followed. Once a load drop occurred, the test was paused and the door of the oven was opened. The crack length was measured and then the door was closed. Unloading and re-heating occurred simultaneously. When the specimen was once again at the test temperature, the loading cycle could begin again.

3.4. Data Reduction

The load-displacement data gathered during each experiment was imported into Excel for data reduction. Loading/unloading cycles were individually separated to examine one at a time. Change in compliance was used to aid in the determination of the first point of nonlinear crack growth. Then, the critical displacement and corresponding critical load for each cycle were determined from the change in compliance plots. Once all cycles were

completed, correction factors were applied and three methods – Modified Beam Theory (MBT), Compliance Calibration (CC), and Modified Compliance Calibration (MCC) – were used to determine the mode I strain energy release rate (G_I). MBT was used when reporting results since it is the most conservative.

As mentioned, G_I values were calculated from MBT, which is outlined in ASTM D 5528-01 [6]. The equation used to calculate G_I was:

$$G_I = \frac{F}{N} \frac{3P\delta}{2b(a + |\Delta|)} \quad (1)$$

where P = load, δ = load point displacement, b = specimen width, a = delamination length, and Δ , F , and N are correction factors. Δ corrects for rotation at the delamination front. Δ can be obtained by plotting the cube root of compliance vs. delamination length, and then measuring the offset of the x-intercept from the origin. F accounts for the shortening of the moment arm and the tilting of the end blocks. N accounts for the stiffening of the specimens by the blocks. Upon completion of data reduction, the results were converted from English to SI units.

4. Results and Discussion

4.1. Interlaminar Fracture Toughness

The average measured interlaminar fracture toughness values are shown in Table 1 and Figure 5 as a function of temperature. The values in Table 1 and Figure 5 exclude the crack initiation values (the reported quantity are averages of crack propagation values only).

Table 1. IM7/977-2 Interlaminar Fracture Toughness Results

8-ply IM7/977-2 [0 ₃ /+3/-3/0 ₃]		16-ply IM7/977-2 [0 ₇ /+3/-3/0 ₇]	
Temperature °C (°F)	G _I J/m ² (lb/in)	Temperature °C (°F)	G _I J/m ² (lb/in)
-189.5 (-309.1)	241.9 (1.382)	-191.0 (-311.7)	266.4 (1.521)
26.1 (78.9)	297.3 (1.698)	21.5 (70.7)	316.4 (1.806)
N/A	N/A	94.3 (201.8)	390.0 (2.227)
157.9 (316.1)	577.0 (3.295)	165.1 (329.1)	709.4 (4.051)

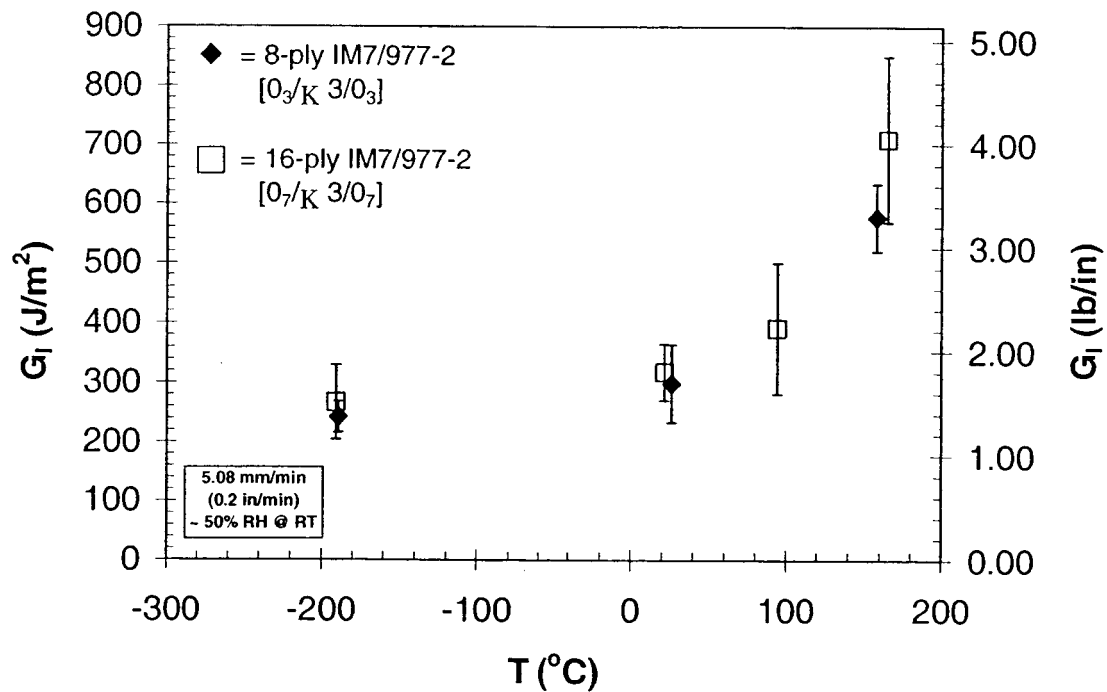


Fig. 5. IM7/977-2 Interlaminar fracture toughness for thick and thin specimens

Notice that the toughness increased with increasing temperature. Interestingly, there was not a large drop in toughness between room temperature and cryogenic. As the

temperature is increased above room temperature, the polymer matrix becomes more ductile and is able to withstand larger strains.

At cryogenic temperatures, the composite becomes stiffer. Previous research by the authors [7] have shown that the strength and stiffness of the resins increase with decreasing temperatures down to cryogenic temperatures. However, the toughness, as measured by the area under the stress-strain curve, decreases with lowering temperatures. This would imply that the stress required to initiate a crack/delamination in the composite might be higher at lower temperatures since the strength of the matrix is higher. However, once the crack/delamination is initiated it will grow more rapidly at the lower temperature because the matrix toughness is lower. Therefore, propagation fracture toughness values would be lower than the initiation. This can be visually seen from the delamination resistance curves discussed in the following section.

Thickness did not significantly affect toughness until 93 °C (200 °F), when the thick specimens showed slightly higher toughness than the thin specimens. One possible explanation for this observation is that the 16-ply specimens were stiffer than the 8-ply due to the increased thickness. The adherend thickness of a DCB specimen does affect the stress distribution at the delamination front; as discussed by Mangalgi, *et al.* [8].

There appeared to be increased fiber bridging in the elevated temperature specimens compared to the room temperature specimens. In the presence of fiber bridging, more load and energy are required to break the fibers (which act as stiffeners preventing crack growth) to allow the crack to propagate. Some fiber bridging was observed in spite of having the +/- 3° layers on either side of the delamination starter insert.

4.2. Delamination Resistance Curves

The delamination resistance curves for the 8-ply and 16-ply specimens at cryogenic temperature are shown in Figure 6. All plots include all crack growth measurements (initiation and propagation). The purpose of the delamination curves is to predict the stability of crack growth. Favorable resistance curves (R-curves) have a positive slope, and unfavorable R-curves have a negative slope. In other words, as the crack length increases, one would want the toughness to increase. This means that the crack would require more energy to propagate. Thus, it would be harder for a delamination to fail catastrophically.

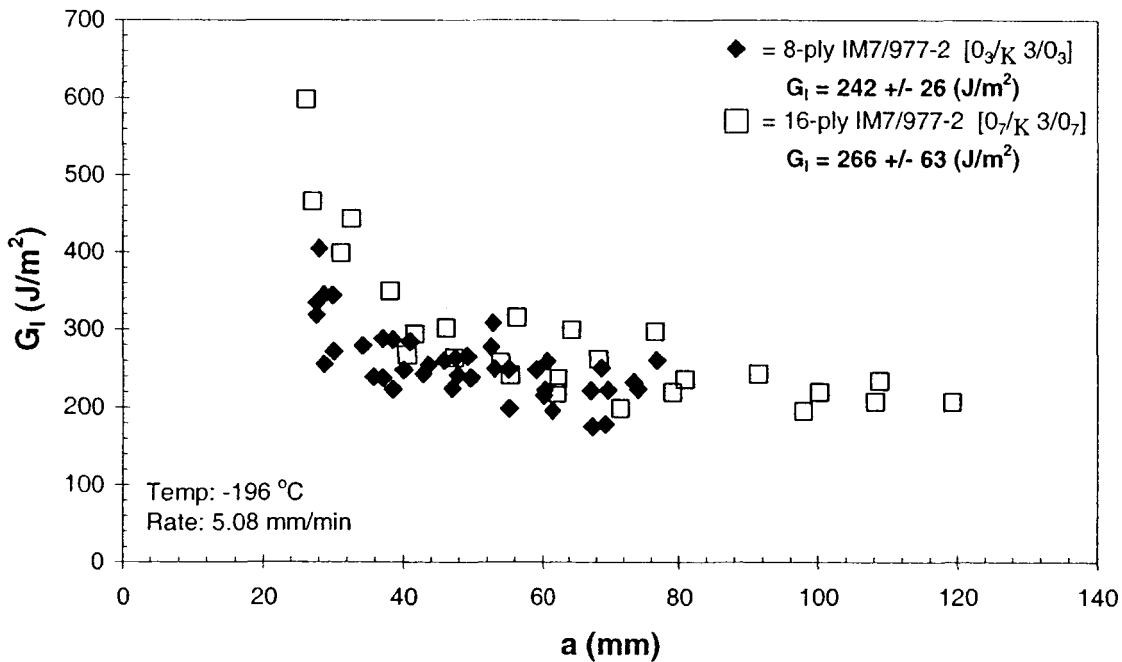


Fig. 6. Cryogenic Temperature (-196 °C) Delamination Resistance Curve

As one can see from Figure 6, the delamination resistance curves for 8-ply and 16-ply at cryogenic temperatures are similar with little variation. All the data points appear to follow

the same trend and in some cases, fall on top of one another. This was very encouraging since the authors were concerned with the difficulty in testing while submerged in LN₂. The trends displayed in the figure are showing a slight negative slope, which would be considered unfavorable. This means that there is increasingly less energy required for crack extension. This makes sense since the polymer matrix is brittle at this temperature; requiring little load to cause cracks to grow. Also, essentially no fiber bridging was noted at this temperature. The initiation values are large compared to propagation and propagation values tend to decrease as crack length increases. Reiterating the aforementioned, a large amount of energy is required for a crack to start, but once it has formed, it propagates rapidly and with little required energy. A sudden stick-slip growth was observed for cryogenic temperature testing, which actually made data analysis easy and accurate. Figure 7 shows evidence of the hackles associated with the stick-slip propagation at the cryogenic temperatures. These hackles were not evident at higher temperatures.

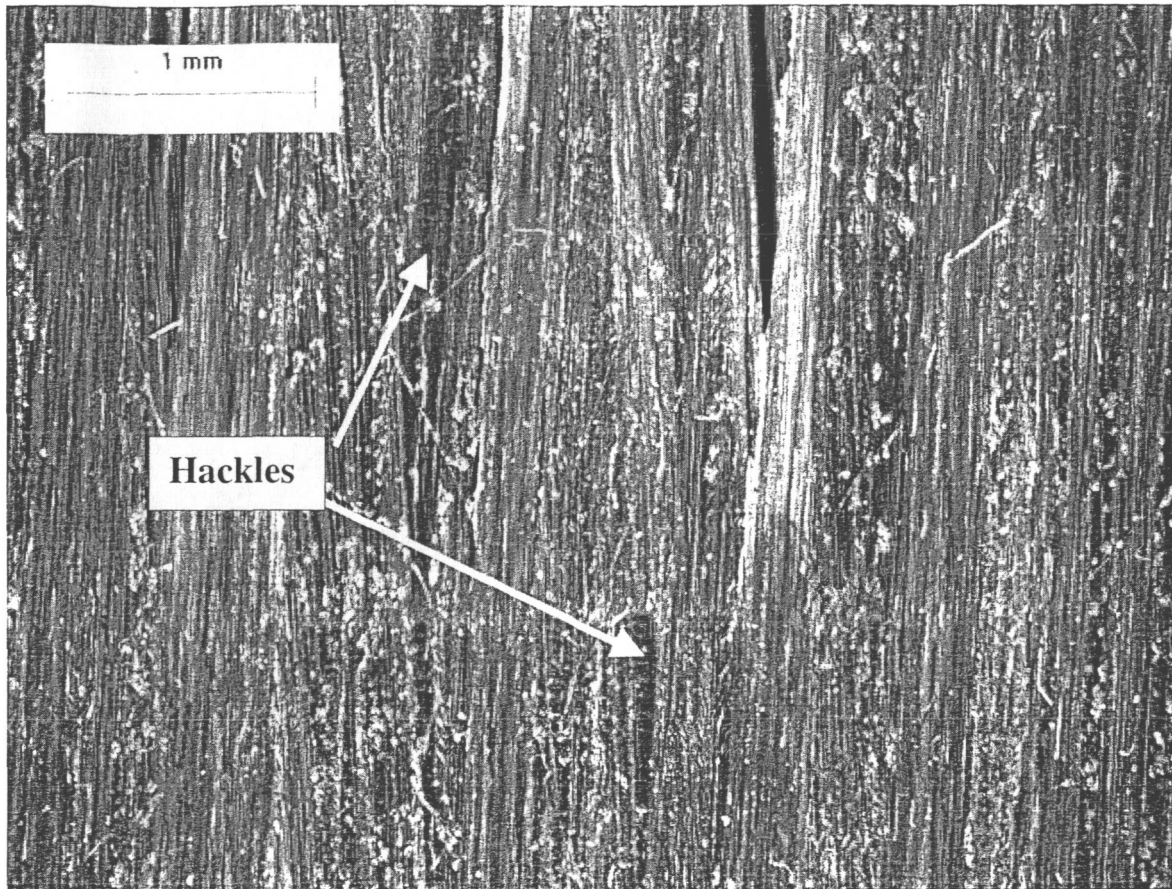


Fig. 7. Fracture surface of a 16-ply specimen tested at $-196\text{ }^{\circ}\text{C}$. Hackles are evident on the surface indicating a brittle matrix fracture.

As indicated in Figure 8, at room temperature, the delamination resistance curves for 8-ply and 16-ply specimens overlap each other. The 8-ply specimens have a large initiation value, and then tend to have a slight decreasing trend for the propagation values. Similarly, the 16-ply specimens have a large initiation value, but then have a relatively flat (if not slight positive) trend. A positive slope would be deemed favorable since that would indicate more energy would be necessary for a crack to propagate throughout the laminate.

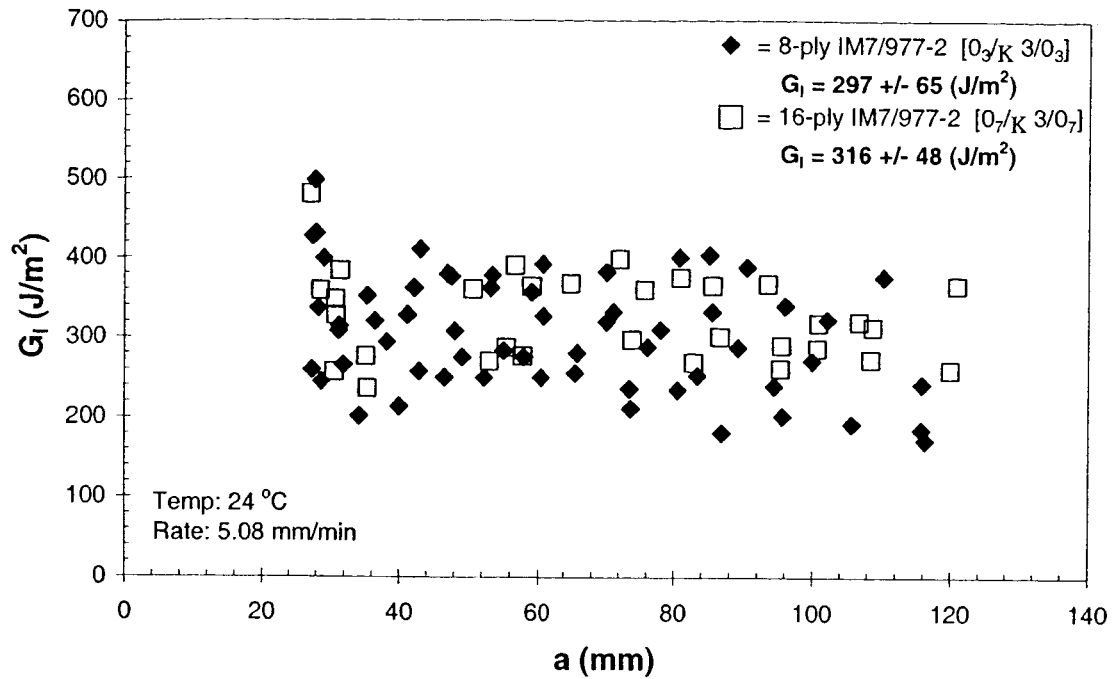


Fig. 8. Room temperature (24 °C) delamination resistance curves

Figure 9 shows the delamination resistance curves for the intermediate 93 °C (200 °F) temperature for the 16-ply specimen only. Notice the large scatter in data, much of which indicates a positive slope. Due to the limited number of specimens, additional tests to possibly reduce the large scatter were not possible. The results at this temperature begin to show a significant increase in toughness with increasing crack length.

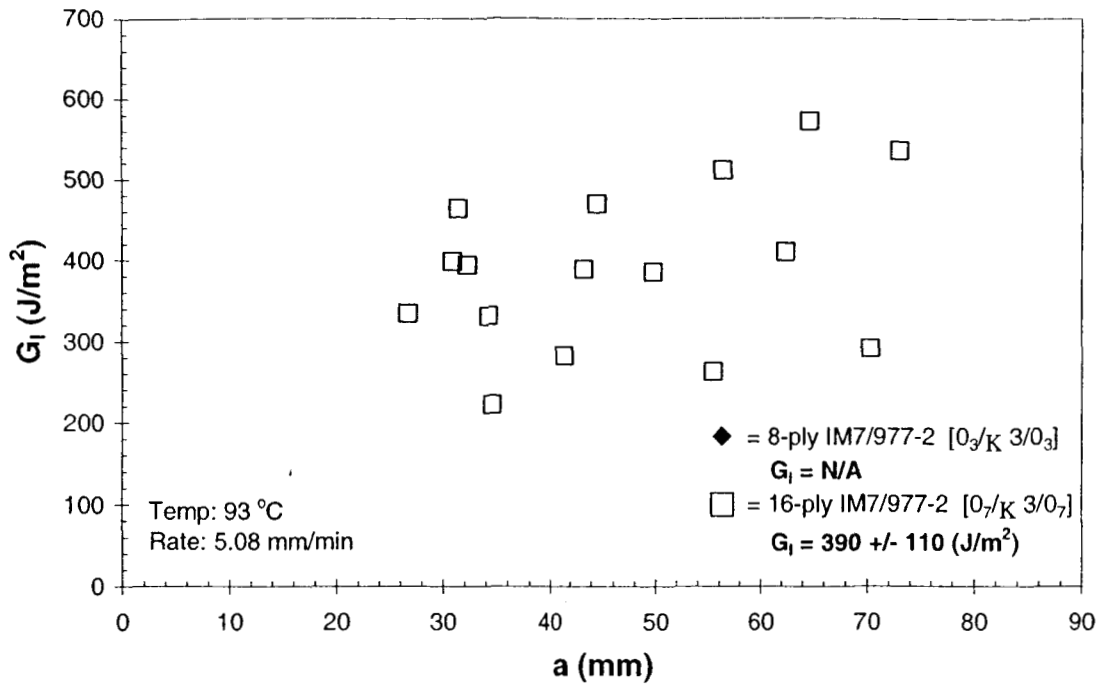


Fig. 9. Intermediate temperature (93 °C) delamination resistance curves

The R-curves in Figure 10 indicate a higher toughness for the thick (16-ply) specimens compared to the thin (8-ply) specimens at elevated temperature, 160 °C (320 °F). At this temperature, all toughness values for the thick specimens exceed those of the thin specimens beyond a crack length of 3.6 cm (1.4 in). This is consistent with the observations made in Ref [8]. “The thickness of the adherend in double cantilever beam specimens influences the measured static fracture toughness... The thicker the adherend the higher the static toughness.” This was attributed to the thicker adherend being stiffer and creating a longer plastic zone at the crack/delamination tip. In addition, fiber bridging was observed in the 16-ply specimens at this temperature, which could also contribute to this observation. Notice that the toughness values at this temperature are significantly greater than the other 3 test temperatures.

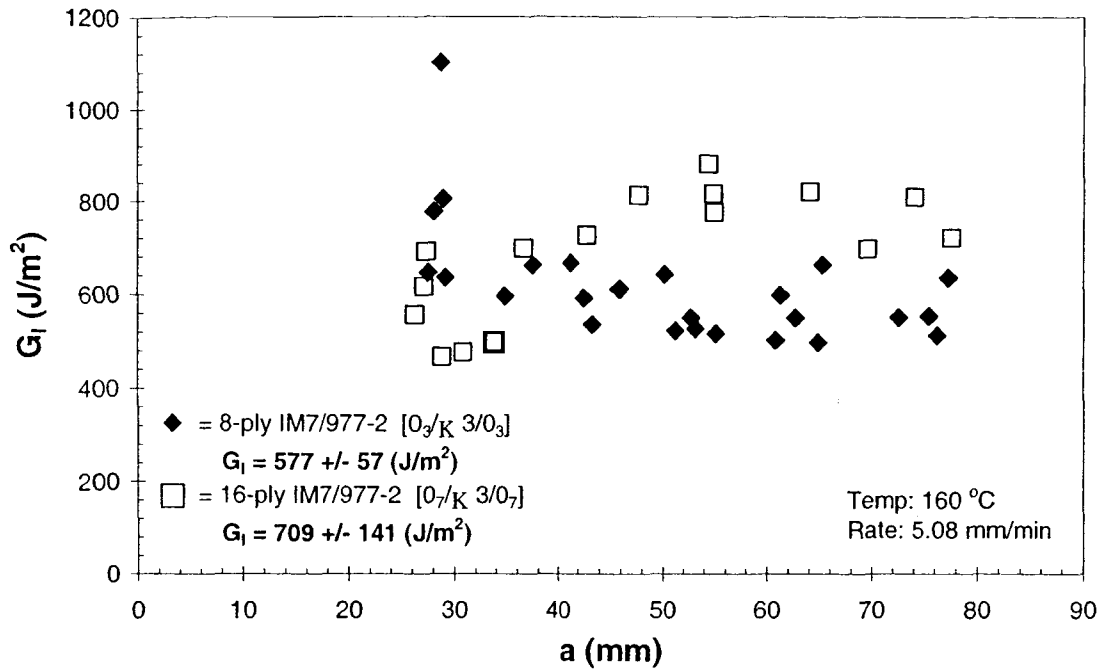


Fig. 10. Elevated temperature (160 °C) delamination resistance curves

The authors also examined the feasibility of testing at temperatures exceeding 160 °C (320 °F) to “push the material to its limits.” A couple tests were attempted at 177 °C (350 °F) and 204 °C (400 °F), however, the material could not withstand those temperatures. Therefore, crack initiation and propagation values were unable to be determined for these tests. In many cases, only 1 or 2 data points could be gathered prior to specimen breakdown. It appeared that the matrix failed at these temperatures, which is consistent with its published usage temperatures [3].

4.3. Load-Displacement Curves

As the test frame's crosshead was moving at 5.08 mm/min (0.2 in/min), the data acquisition system was simultaneously recording displacement and applied load. Plots of load vs. displacement (crosshead) were generated to aid in determining crack growth. Representative load-displacement curves for both types of specimens (8-ply and 16-ply "unidirectional") at each test temperature are shown in Figures 11-17.

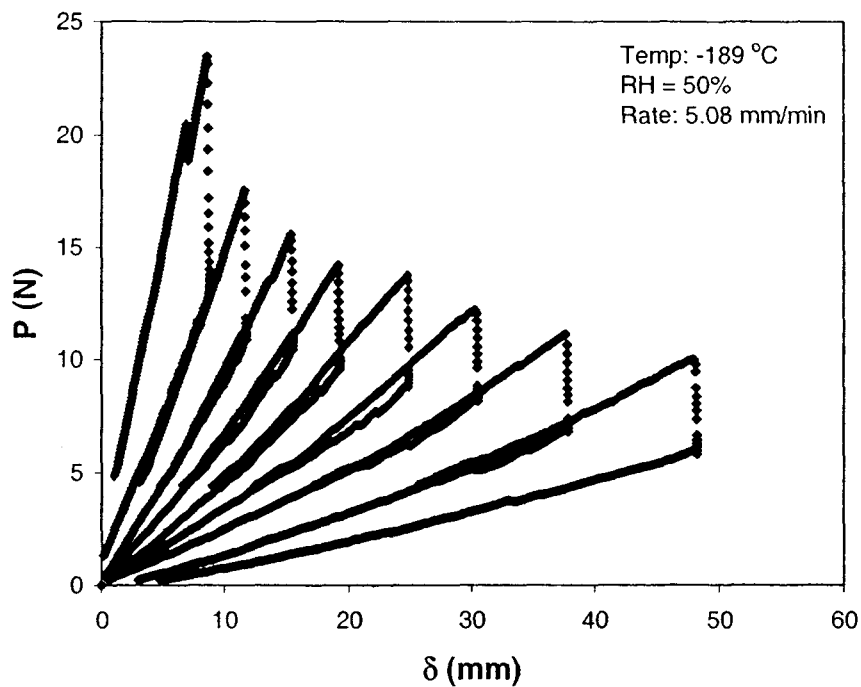


Fig. 11. 8-ply cryogenic temperature load-displacement curve

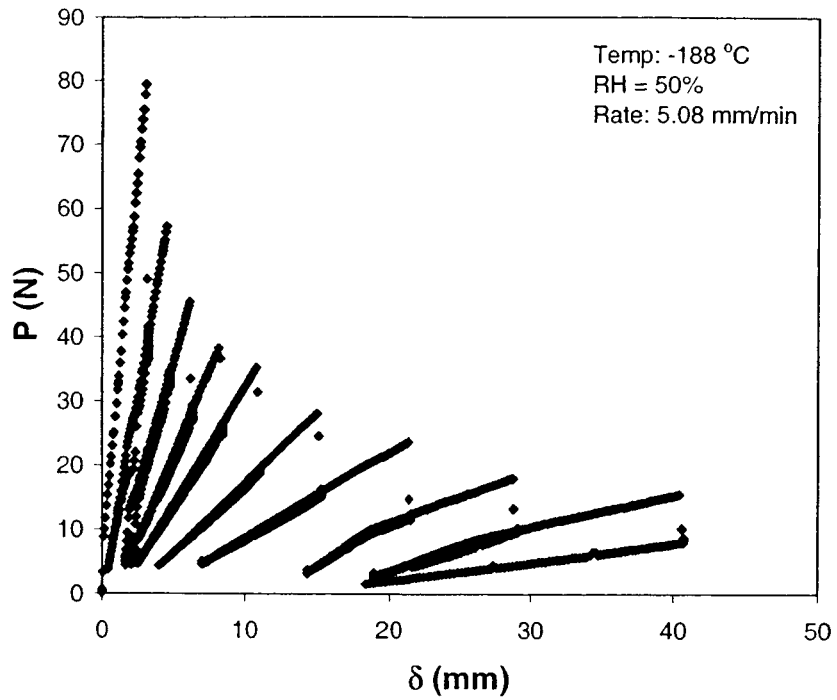


Fig.12. 16-ply cryogenic temperature load-displacement curve

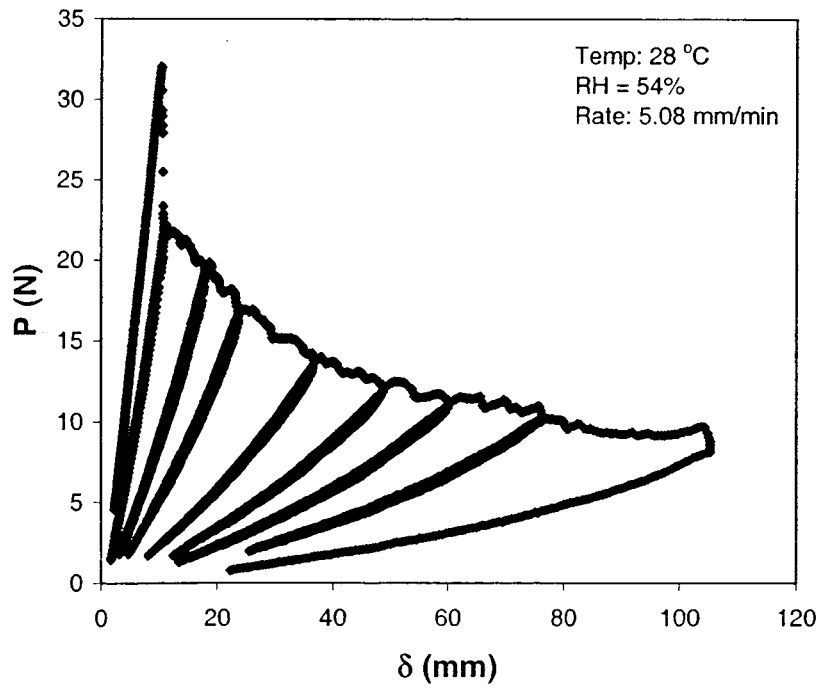


Fig. 13. 8-ply room temperature load-displacement curve

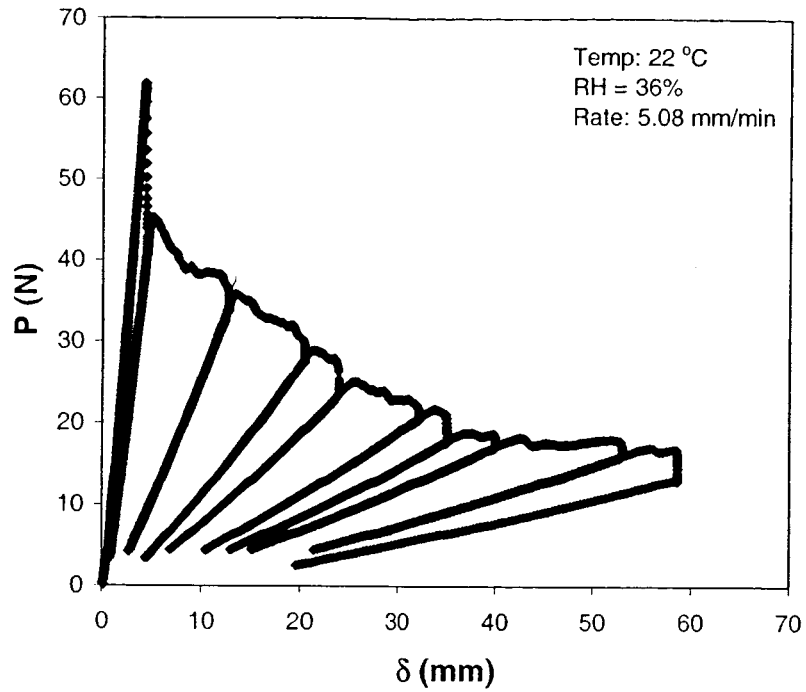


Fig. 14. 16-ply room temperature load-displacement curve

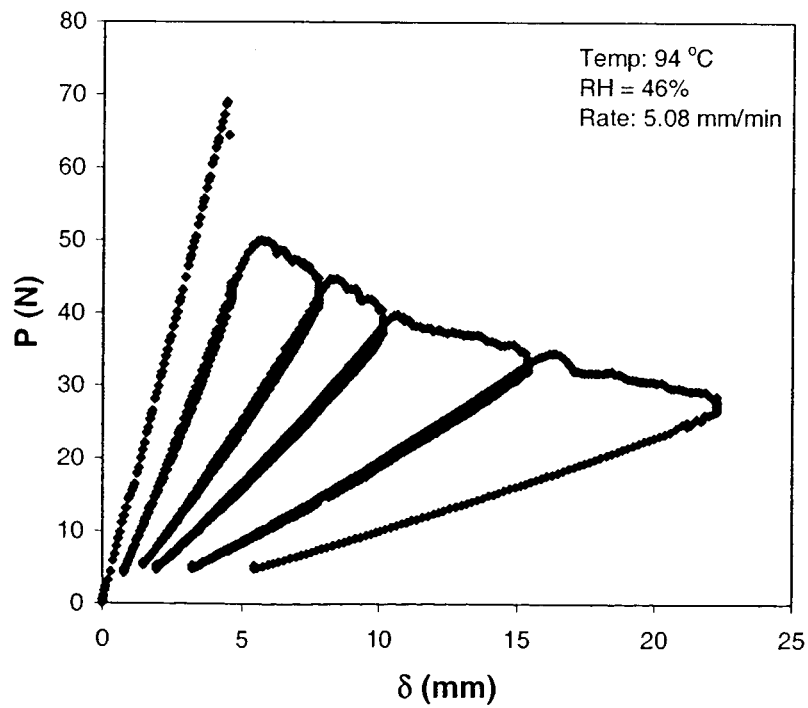


Fig. 15. 16-ply intermediate temperature load-displacement curve

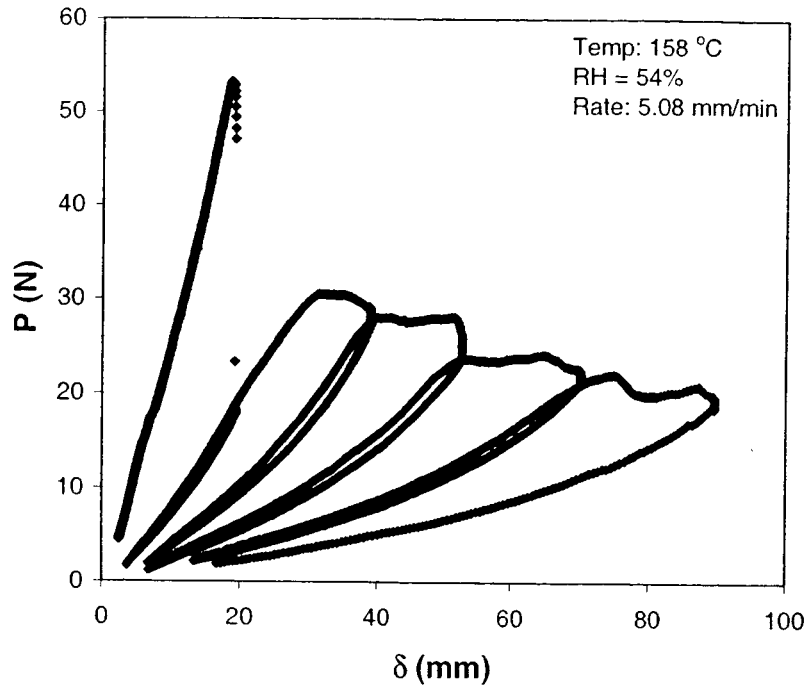


Fig. 16. 8-ply elevated temperature load-displacement curve

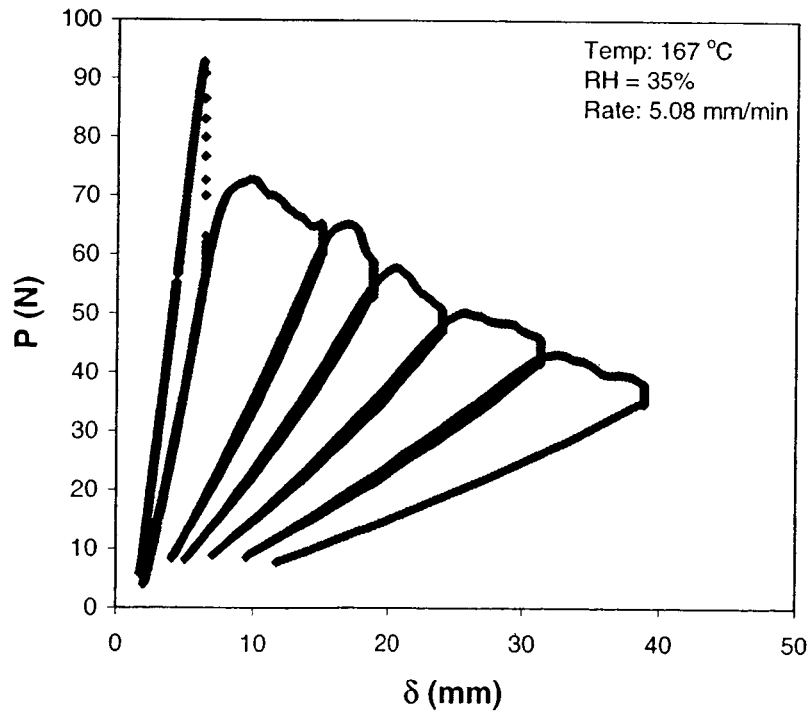


Fig. 17. 16-ply elevated temperature load-displacement curve

At first glance, it is easy to see the differences in trends among the 7 diagrams. The two cryogenic curves (Figures 11 and 12) are drastically different from the others; a stick-slip crack growth pattern. The specimen loaded linearly, and then would suddenly “pop” emitting a distinctive sound and showing an abrupt drop in applied load. Comparing this to the other curves, it is apparent that the tests at the three other temperatures exhibit a non-linear loading phase when the crack begins to propagate, a more stable growth. Also, observe that the loading curves at 93 °C (200 °F) and 160 °C (320 °F) have a more pronounced non-linear phase. This makes data reduction more difficult since it is unclear when a crack began to propagate. Change in compliance was relied upon to determine when crack extension occurred, as recommended in ASTM Standard D 5528-01[6]. However, experiments at these two temperatures still exhibited large scatter.

From Figures 13 and 14, one can see that the room temperature $P-\delta$ trends differ from one another in that the loads are approximately double, presumably due to the specimen thickness being doubled. Both indicate a more stable crack growth compared to Figures 11 and 12 (cryogenic testing), since there is not an abrupt drop in load. Figures 15 through 17 show the same stable, nonlinear behavior as the crack grows. Again, one can see the lower level of loading required with the thinner adherend specimen.

5. Conclusions

The objective of this work was to determine the mode I interlaminar fracture toughness of “unidirectional” 8-ply and 16-ply IM7/977-2 specimens at rather extreme temperatures. Tests were performed at -196 °C (-320 °F), 22 °C (-72 °F), 93 °C (200 °F) and 160 °C (320

°F). Low temperature testing was completed while the specimen was submerged in a liquid nitrogen bath. High temperature testing was completed in a temperature-controlled oven.

At cryogenic and room temperature, thickness had little effect on G_{Ic} , as indicated by the close average values as well as the overlapping delamination resistance curves. This is attributed to the brittle nature of the matrix at these temperatures. At the intermediate temperature, 93 °C (200 °F), the 16-ply specimen results show the beginning of a pronounced increase in toughness. At 160 °C (320 °F), the 16-ply specimens resulted in higher G_{Ic} values than the 8-ply specimens. In addition, the toughness values at this temperature are much larger than at the other temperatures examined. Also, the delamination resistance curves do not overlap beyond the “pop-in” initiation value and first propagation value. Beyond a crack length of 3.6 cm (1.4 in), all 16-ply values exceed all 8-ply values, clearly showing a significant increase in toughness for the 16-ply specimens. Some of this increase in toughness may be attributed to observed fiber bridging in the 16-ply specimen.

The authors developed confidence in their cryogenic testing procedure and equipment. The interlaminar fracture toughness results obtained for both specimen thicknesses at LN₂ were almost identical. Lastly, the novel bolted loading block method developed is a robust method for attaching mechanical loading blocks to DCB specimens. However, the “wedged U-clip” method appears to be an accurate alternative method (provided that the initial flaw from the Teflon insert is not exceeded) in situations when the DCB specimen’s thickness does not allow for the bolted method.

It is encouraging that the IM7/977-2 composites did not show a significant decrease in interlaminar fracture toughness when tested at -196°C when compared to room temperature results.

Acknowledgements

The authors would like to thank the project's two technical monitors Drs. Brian Jensen and Erik Weiser at NASA Langley Research Center in Hampton, VA. This work was performed under NASA Grant NAG-1-02003. In addition, Beth Saltysiak at Lockheed-Martin in Marietta, GA deserves thanks for assisting in the fabrication of the two composite panels. Also, Drew Smith at NASA Marshall Space Flight Center in Huntsville, AL deserves recognition for his role in the approval and sharing information regarding NGLT and RLV technology. Lastly, Tod Palm and Jim Bohlen at Northrop-Grumman in El Segundo, CA require thanks for their time invested in providing information and materials.

References

1. Cast, J, Amatore, D. 1996. Delta Clipper Rolls Out; Flight Tests to Begin in May. NASA Press Release #96-51, March 15, 1996.
2. Hexcel. IM7 Carbon Fiber Product Data.
<http://www.hexcelfibers.com/NR/rdonlyres/exq6f5qnsmaf7fvvhghvx7ohr2gchoigvuctqyjezu4o3ttt7akmtcw475bqf3ifcrfx6abkycglxosixojqf7vv23h/im7.pdf>
3. Cytec. Cycom 977-2 Toughened Epoxy Resin.
<http://www.cytec.com/business/EngineeredMaterials/Datasheets/CYCOM%20977-2.pdf>
4. Johnson, W S, Mangalgi, P D. Investigation of Fiber Bridging in Double Cantilever Beam Specimens. Journal of Composites Technology & Research 1987; 9(1):10-13.

5. Melcher, R J, Johnson, W S. Fracture Mechanics of Adhesively Bonded Polymer Matrix Composites in Cryotank Environments. Proceedings of the 14th International Conference on Composite Materials, July 14-18, 2003, SME Publishers.
6. D 5528-01. Standard Test Method for Mode I Interlaminar Fracture Toughness of Unidirectional Fiber-Reinforced Polymer Matrix Composites. Reprinted from the *Annual Book of ASTM Standards*, American Society for Testing and Materials, 1999.
7. Pavlick, M M, Johnson, W S. Mode I Fracture Toughness of Advanced Polymers in a Cryotank Environment. Proceedings of the American Society for Composites/ASTM-D30 Joint 19th Annual Technical Conference. Ed. E. Armanios. October 2004.
8. Mangalgiri, P D, Johnson, W S, Everett, R A, Jr. Effect of Adherend Thickness and Mixed-Mode Loading on Debond Growth in Adhesively Bonded Composite Joints. *Journal of Adhesion* 1987; 23(1):263-288.